Equivalent Circular Defect Model of Real Defect Outlines in the IC Manufacturing Process

Xiaohong Jiang, Yue Hao, *Senior Member, IEEE,* and Guohua Xu

***Abstract*— For efficient yield prediction and inductive fault analysis of integrated circuits (IC's), it is usually assumed that defects related to photolithography have the shape of circular discs or squares. Real defects, however, exhibit a great variety of shapes. This paper presents an accurate model to characterize those real defects. The defect outline is used in this model to determine an equivalent circular defect such that the probability that the circular defect causes a fault is the same as the probability that the real defect causes a fault, so a norm is available which can be used to determine the accuracy of a defect model, and thus estimate approximately the error that will be aroused in the prediction of fault probability of a pattern by using circular defect model. Finally, the new model is illustrated with the real defect outlines obtained by optical inspection.**

***Index Terms*—Equivalent circular defect, fault-probability, IC defect, yield.**

I. Introduction

THE frequency of defects and the defect size distribution are important data for inductive fault analysis and yield prediction [1]. Defect statistics are also used for yield estimation [2], [3], integrated circuit (IC) manufacturing process optimization [4], and test pattern generation [5]. The probability that a defect causes a fault in the implemented electrical network depends on the spatial distribution of defects and the distribution of the defect sizes. In order to avoid the time-consuming computations required by complex defect shapes, defects are usually modeled as circular discs [3], [6]–[9], or squares [10]. However, real defects show a great variety of different shapes. Fig. 1 shows some real defect shapes.

Few papers available deal with the question of how to determine a proper diameter of the circular disc model for real defect data. If the diameter of the circular disc model is determined as the maximum extension of the real defect (see Fig. 2 [11]), the probability of causing a fault would be estimated too high. Otherwise, if the diameter of the circular disc model is determined as the minimum extension of the real defect, the probability of causing a fault would be estimated too low.

This paper presents an accurate theoretical model of how to determine an equivalent diameter of the circular defect for real defect data such that the probability that the circular defect causes a fault is the same as the probability that the real defect causes a fault, so a norm is available which can be used to determine the accuracy of a defect model, and thus estimate approximately the error that will be aroused in the prediction of fault probability of a pattern by using the circular defect model. Finally, the new model is illustrated with the real defect outlines obtained by optical inspection.

This paper is organized as follows. Section II starts with the characterization of the probability that the circular defect causes a fault and then describes our approach to determine the equivalent diameter of a circular defect for real defect data. Section III gives experimental results and discussion. Section IV concludes the paper.

Manuscript received December 3, 1996; revised October 6, 1997.

X. Jiang and Y. Hao are with the Microelectronics Institute, Xidian University, Xi'an 710071, Shaanxi, China (e-mail: meicad@xidian.edu.cn).

G. Xu is with the School of Electronic Mechanics, Xidian University, Xi'an 710071, Shaanxi, China.

Publisher Item Identifier S 0894-6507(98)05884-9.

II. Defect Outline Modeling

A. Probability of a Circular Defect to Cause a Fault

Consider multiple patterns consisting of n conductors, each of width w and length L, with separation s_j between the jth and $(j+1)$th conductor as shown in Fig. 3.

Since in general the grids used for layouts are orthogonal, the analysis of the open circuits or short circuits fault caused by local defects in the pattern shown in Fig. 3 lays the foundation for analyzing the open circuits or short circuits fault caused by a local defect in the general pattern. Assume for simplicity that an open circuit results only if the pattern is completely broken. In order to get the probability that a defect causes a fault in the pattern of Fig. 3, we first make the following assumption.

Assumption: Defects falling in the pattern of Fig. 3 are uniformly distributed in the pattern.

Then the following Lemma 1 can be obtained [3].

Lemma 1: The probability $F^o(R, w, s_1, \cdots, s_{n-1}, x)$ that a circular defect with a diameter R causes the open circuits fault in the pattern shown in Fig. 3 is given by

$$F^o(R, w, s_1, \cdots, s_{n-1}, x) = \begin{cases} 0, & 0 \le R \le X_0 \\ \sum_{j=0}^{n-1} F_j^o(R, w, s_1, \cdots, s_{n-1}, x), & X_0 \le R \le X_n \\ 1, & X_n \le R \le R_M \end{cases} \quad (1)$$

where, as shown in (2) at the bottom of the next page, $X_0 = w$, $X_j = s_j + 2X_0$, $s_0 = -X_0$, $s_n = x - nX_0 - \sum_{i=1}^{n-1} s_i$, R_M is the maximum value possible of defect diameters, and w, x, and $s_1, s_2, \cdots, s_{n-1}$ is defined in Fig. 3, $j = 0, 1, \cdots, n-1$.

For short circuits fault, we get similar result as shown in the following lemma.

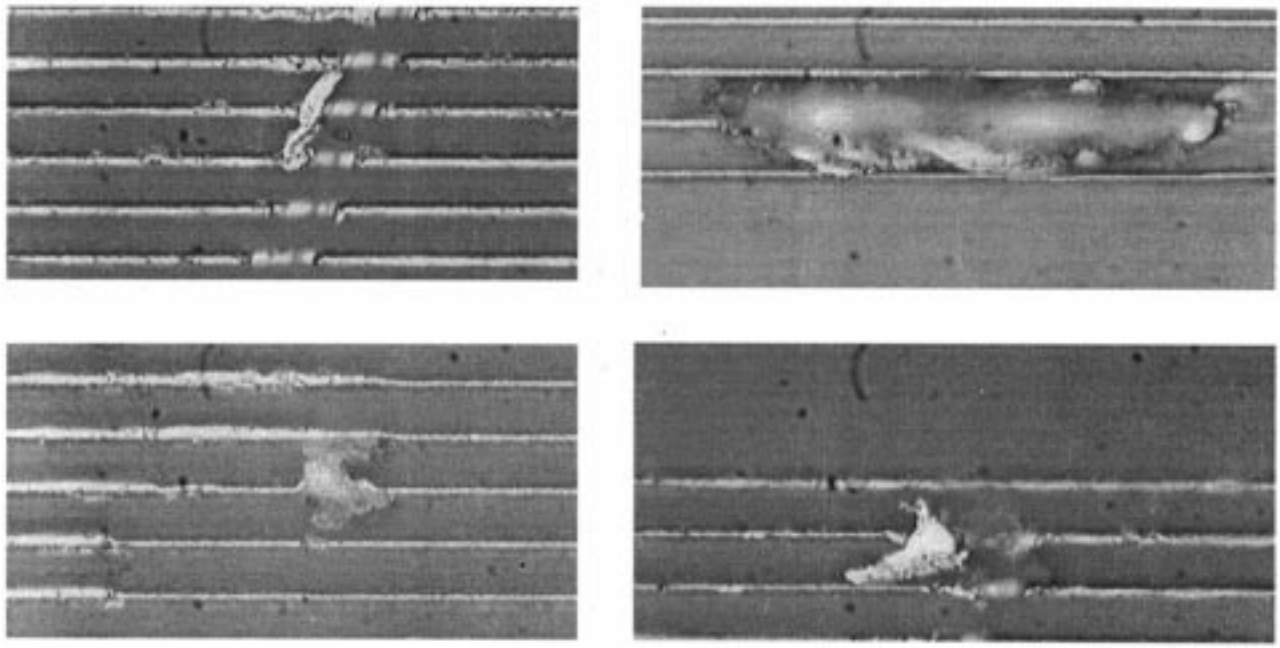

Fig. 1. Real defect shapes.

$$F_j^o(R, w, s_1, \cdots, s_{n-1}, x) = \begin{cases} \dfrac{n(R-w) - (1-\delta_{j0})\sum_{i=1}^{j}(R-x_i)}{x}, & R \in [X_j, X_{j+1}] \\ 0, & R \notin [X_j, X_{j+1}] \end{cases} \tag{2}$$

$$F^s(R, w, s_1, \cdots, s_{n-1}, x) = \begin{cases} 0, & 0 \le R \le s_1 \\ \sum_{j=1}^{n-1} F_j^s(R, w, s_1, \cdots, s_{n-1}, x), & s_1 \le R \le s_n \\ 1, & s_n \le R \le R_M \end{cases} \tag{3}$$

where

$$F_j^s(R, w, s_1, \cdots, s_{n-1}, x) = \begin{cases} \dfrac{\sum_{i=1}^{j}(R-s_i) - (1-\delta_{j1})\sum_{i=1}^{j-1} M_{i,i+1}(R, w, s_i, s_{i+1}) - N(R, w, s_1, \cdots, s_{n-1}, x)}{x}, & R \in [s_j, s_{j+1}] \\ 0, & R \notin [s_j, s_{j+1}] \end{cases} \tag{4}$$

$$M_{k,k+1}(R, w, s_k, s_{k+1}) = \begin{cases} R - s_k - s_{k+1} - w, & R > w + s_k + s_{k+1} \\ 0, & R \le w + s_k + s_{k+1} \end{cases} \quad k = 1, \cdots, n-2,\ j = 1, 2, \cdots, n-1 \tag{5}$$

$$N(R, w, s_1, \cdots, s_{n-1}, x) = \begin{cases} \dfrac{R - 2(s_1 + w + \zeta)}{2}, & R > 2(w + s_1 + \zeta) \\ 0, & R \le 2(w + s_1 + \zeta) \end{cases} \tag{6}$$

$$\zeta = \frac{x - nw - \sum_{i=1}^{n-1} s_i}{2}, \quad s_n = 2(w + s_{n-1} + \zeta). \tag{7}$$

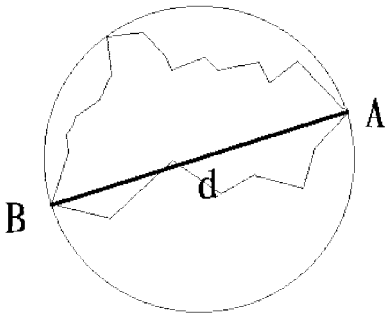

Fig. 2. Circular disc model.

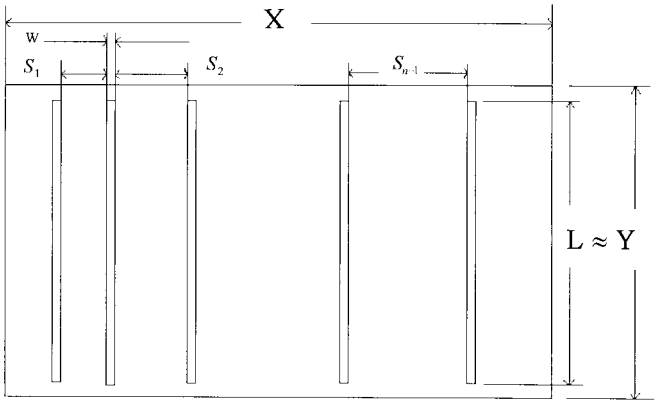

Fig. 3. Multiple patterns each of width w and length $L \approx Y$ with space s_j between the jth and $(j+1)$th pattern, where $s_j \leq s_{j+1}, j = 1, 2, \cdots, n-1$.

Lemma 2: The probability $F^s(R, w, s_1, \cdots, s_{n-1}, x)$ that a circular defect with a diameter R causes the short circuits fault in the pattern shown in Fig. 3 is given by (3)–(7), shown at the bottom of the previous page.

B. The Existence of Local Equivalent Circular Defect (LECD) and the Characterization of Its Size

First, we give the following definition.

Definition 1) Local Equivalent Circular Defect: For a specified pattern (e.g., the multiple patterns shown in Fig. 3), a circular defect is defined as the local equivalent circular defect of a real defect if the probability that the circular defect causes a fault in the pattern is the same as the probability that the real defect causes a fault in the pattern.

Definition 2) Directional Extension and Orientation of a Real Defect: For a real defect, the maximum possible extension of the real defect between two parallel straight lines, which corresponds to a direction and touches the defect is called the directional extension of the real defect in the direction. As can be seen in Fig. 4, the directional extension of the defect (dependent on the angle θ) corresponds to the distance $d(\theta)$. The orientation of the defect is defined as the angle where $d(\theta)$ reaches its minimum.

Then for the multiple patterns shown in Fig. 3, the probability p^s that a real defect causes a short circuit fault and the probability p^o that the defect causes an open circuit fault can

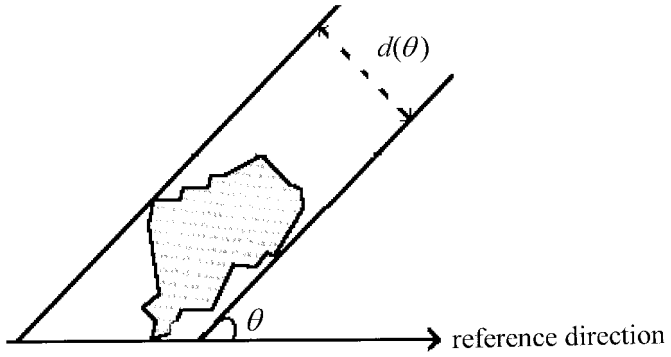

Fig. 4. Measurement of real defect extension.

be expressed as

$$p^s = \int_0^{\pi} F^s(d(\theta), w, s_1, \cdots, s_{n-1}, x) f(\theta)\, d\theta \tag{8}$$

$$p^o = \int_0^{\pi} F^o(d(\theta), w, s_1, \cdots, s_{n-1}, x) f(\theta)\, d\theta \tag{9}$$

where $F^s(d(\theta), w, s_1, \cdots, s_{n-1}, x)$ is the probability that the real defect causes a short circuit fault in the multiple patterns of Fig. 3 when its orientation is θ, $F^o(d(\theta), w, s_1, \cdots, s_{n-1}, x)$ is the probability that the real defect causes an open circuit faults in the multiple patterns of Fig. 3 when its orientation is θ, the probability density function of the orientation angle θ is $f(\theta)$, which holds

$$\int_0^{\pi} f(\theta)\, d\theta = 1. \tag{10}$$

From the above definitions and expressions we have the following results.

Theorem 1. Existence of LECD: For a real defect falling in the multiple patterns of Fig. 3, there exists at least one LECD such that the probability that the LECD causes a fault (short circuit faults or open circuits faults) is just the same as the probability that the real defect causes a fault in the same pattern. In other words, the LECD of the real defect is existent. Especially, when p^s and p^o satisfy $0 < p^s < 1$, $0 < p^o < 1$, the LECD is existent and unique. The proof of Theorem 1 can be found in Appendix A.

Based on the existence of LECD, the size of LECD can be characterized as follows.

Theorem 2: If a real defect falling in the multiple patterns of Fig. 3 may cause a short circuit fault, then the diameter R^* of its LECD can be determined by solving the following equation:

$$\begin{aligned} &F^s(R^*, w, s_1, \cdots, s_{n-1}, x) \\ &\quad = \sum_{j=1}^{n-1} \frac{1}{x} \left[\lambda_j \int_{A_j} d(\theta) f(\theta)\, d\theta + \mu_j \int_{A_j} f(\theta)\, d\theta \right] \\ &\qquad + \int_{A_n} f(\theta)\, d\theta \end{aligned} \tag{11}$$

where

$$\lambda_j = j - (1-\delta_{j1}) \sum_{i=1}^{j-1} \gamma(d(\theta) - s_i - s_{i+1} - w) - \tfrac{1}{2}\gamma(d(\theta) - 2(w + s_1 + \zeta)) \qquad (\theta \in A_j) \quad (12)$$

$$\mu_j = \sum_{i=1}^{j}(-s_i) + (1-\delta_{j1}) \sum_{i=1}^{j-1}(s_i + s_{i+1} + w) \cdot \gamma(d(\theta) - s_i - s_{i+1} - w) + (w + s_1 + \zeta) \cdot \gamma(d(\theta) - 2(w + s_1 + \zeta)) \qquad (\theta \in A_j) \quad (13)$$

$$\gamma(X) = \begin{cases} 0, & X \le 0 \\ 1, & X > 0 \end{cases}$$

$$A_j = \{\theta | s_j \le d(\theta) \le s_{j+1}\}, \quad j = 1, 2, \cdots, n-1, \quad A_n = \{\theta | s_n \le d(\theta) \le R_M\}.$$

Especially, if there exists $j^*(1 \le j^* \le n-1, j^* \in N)$ such that $\min_\theta d(\theta) = s_{j^*}$, $\max_\theta d(\theta) = s_{j^*+1}$ and if the distribution of the orientation angle θ is uniform in $A = \{\theta | 0 \le \theta \le \pi\}$, then it is easy to see that the unique solution of (11) is

$$R^* = \frac{1}{\pi}\int_0^\pi d(\theta)\, d\theta = \frac{1}{\pi}\int_\psi^{\psi+\pi} d(\theta)\, d\theta \qquad (14)$$

where Ψ is an arbitrary but fixed direction. This is the result obtained in [11], and it is only a special case of the above result. The proof of Theorem 2 is given in Appendix B.

Based on the above conclusion, we have the following corollary.

Corollary 1: If a real defect falling in the multiple patterns shown in Fig. 3 may causes an open circuit fault, then the diameter R^* of its LECD is determined by solving the following equation:

$$F^o(R^*, w, s_1, \cdots, s_{n-1}, x) = \sum_{j=0}^{n-1} \frac{1}{x}\left[\upsilon_j \int_{B_j} d(\theta) f(\theta)\, d\theta + \omega_j \int_{B_j} f(\theta)\, d\theta\right] + \int_{B_n} f(\theta)\, d\theta \qquad (15)$$

where

$$\upsilon_j = n - (1-\delta_{j0}) \times j,$$

$$\omega_j = -nw + (1-\delta_{j0}) \sum_{i=1}^{j} X_i \qquad (16)$$

$$B_j = \{\theta | X_j \le d(\theta) \le X_{j+1}\}, \quad j = 0, 1, 2, \cdots, n-1, \qquad B_n = \{\theta | X_n \le d(\theta) \le R_M\}. \qquad (17)$$

Especially, if there exists $j^*(0 \le j^* \le n-1, j^* \in N)$ such that $\min_\theta d(\theta) = X_{j^*}$, $\max_\theta d(\theta) = X_{j^*+1}$ and if the distribution of the orientation angle θ is uniform in $A = \{\theta | 0 \le \theta \le \pi\}$, the unique solution of (20) is

$$R^* = \frac{1}{\pi}\int_0^\pi d(\theta)\, d\theta = \frac{1}{\pi}\int_\psi^{\psi+\pi} d(\theta)\, d\theta \qquad (18)$$

where Ψ is an arbitrary but fixed direction.

C. An Approximate LECD Model

The above analysis indicates that it is the extent function $d(\theta)$ and thus the convex hull (not the actual shape) of a real defect that is important in determining its R^* (and thus the probability the defect cause a fault) in a pattern. In practice, the extent function $d(\theta)$ has to be estimated in a simple way to eliminate the need to keep all the outline data. Then an approximate size of LECD can be obtained by using the estimated extent function. One way is to use $\hat{d}(\theta)$, an elliptical approximation to the extent function $d(\theta)$ [11], to find an equivalent radius, $\hat{R}^*$. That is, to find a roughly equivalent radius to $d(\theta)$ by solving the following equation:

$$F^s(\hat{R}^*, w, s_1, \cdots, s_{n-1}, x) = \int_0^\pi F^s(\hat{d}(\theta), w, s_1, \cdots, s_{n-1}, x) f(\theta) d\theta \qquad (19)$$

or

$$F^o(\hat{R}^*, w, s_1, \cdots, s_{n-1}, x) = \int_0^\pi F^o(\hat{d}(\theta), w, s_1, \cdots, s_{n-1}, x) f(\theta) d\theta \qquad (20)$$

where

$$\hat{d}(\theta) = \frac{d_{\min}}{\sqrt{1 - \left(1 - \left(\frac{d_{\min}}{d_{\max}}\right)^2\right) \cdot \sin^2\theta}},$$

$$d_{\max} = \max_\theta d(\theta), \; d_{\min} = \min_\theta d(\theta).$$

This has the effect of dramatically reducing the amount of data required for each defect [from the entire extent function $d(\theta)$ to just $d_{\max}$ and $d_{\min}$].

III. Experimental Results and Discussions

A. Experimental Results

In order to compare the LECD model developed in this paper with models available, more than 500 real defect samples (several of those samples are shown in Fig. 1) were obtained using a test chip designed with a mature 5 μm technology. The novel test structure design developed in [11] is adopted in the test chip to localize real defects, and then optical measurement equipment is used to detect the details of these real defect. The outlines of these defects are abstracted by using Photo Styler (software for image processing). Only defects of type "extra material" are considered. Based on these outlines, the ratio $d_{\max}/d_{\min}$ and the orientations of these real defects are summarized in Figs. 5 and 6, respectively.

Analysis of Fig. 6 shows that the distribution of the orientation is governed by the probability density function $f((\pi/2), 0.11, 0.40, \theta)$ with $f(\mu, h_0, h, \theta)$ defined as

$$f(\mu, h_0, h, \theta) = \begin{cases} \dfrac{h}{\mu}\theta + h_0 & 0 \le \theta \le \mu \\ -\dfrac{h}{\mu}\theta + h_0 + 2h & \mu < \theta \le 2\mu \end{cases} \qquad (21)$$

where $h > 0$, $h_0 > 0$, $\mu \ge 0$, and $\mu(h + 2h_0) = 1$.

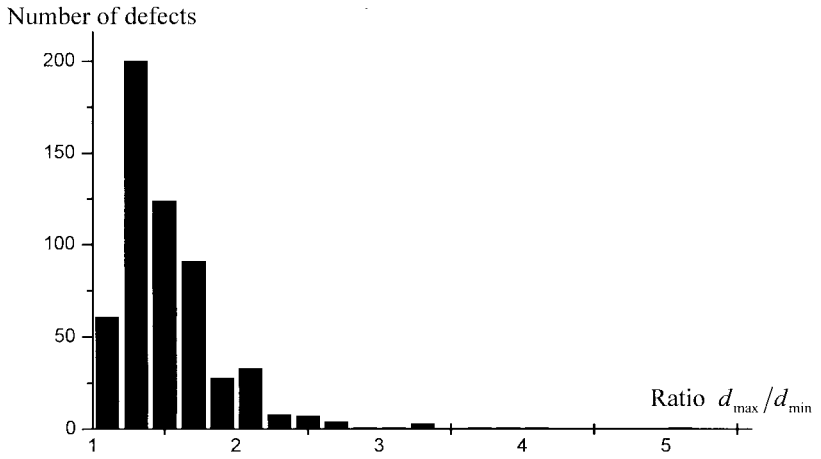

Fig. 5. Distribution of ratio $d_{\max}/d_{\min}$.

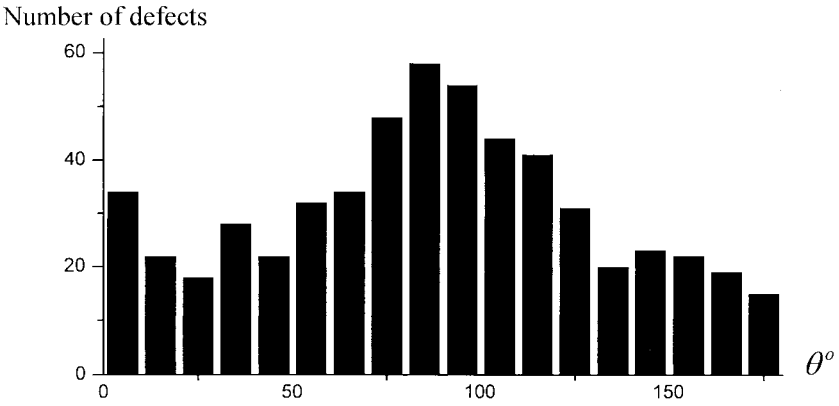

Fig. 6. Distribution of defect orientation.

That is to say, the distribution of defect orientation appears to peak near $\pi/2$. Presumably, the distribution of the orientation should be uniform for $\theta = 0^\circ \cdots 180^\circ$. This may be the result of bias in the procedure used to locate defects. The distribution of $d_{\max}/d_{\min}$ obtained Fig. 5 indicates that the real defects are almost all oblong. Clearly, oblong defects are more likely to cause faults when oriented vertically, and hence angles near $\pi/2$ might be observed with higher frequency. For simplicity, distribution of the orientation is assumed to be uniform for $\theta = 0^\circ \cdots 180^\circ$. From the result and conclusion in Theorem 2, the LECD of these real defects in the two patterns of Fig. 3 (where $s_1 = w = 5$ μm, $x = 23$ μm) are determined. The fault probability kernel of the two patterns of Fig. 3 is shown in Fig. 7.

Figs. 8 and 9 summarize the measured defect size distributions.

In Fig. 8, the left bar of each size interval shows the size distribution of $d_{\max}$ obtained by using the max circle model, the bars in the center represent the size distribution of R^* obtained by using the LECD model which was described in Section II. The right bars show the size distribution of $d_{\min}$ obtained by using the min circle model. In Fig. 9, the left bars show the distribution of $\hat{R}^*$ obtained by using the approximate LECD model, the center bars represent the size distribution of R^*, and the right bars show the distribution of d_{ellip} which, the diameter of a circular defect obtained by using the elliptical model, is approximated by [11]

$$d_{ellip} \approx \frac{1}{2}\sqrt{d_{\min} \cdot d_{\max}} + \frac{d_{\min} \cdot d_{\max}}{d_{\min} + d_{\max}}. \qquad (22)$$

The min circle model, where the diameter is chosen equal to the minimum extension of the defect, predicts a greater number of defects than other models (LECD, elliptical, max circle) in the regions of smaller defect size (about 5 μm); the max circle model, where the diameter is chosen equal to the maximum extension of the defect, predicts greater number of defects than the other models (LECD, elliptical, min circle) in the regions of larger defect size (approximately larger than 10 μm); and the elliptical model represents an intermediate strategy which predicts an intermediate number of defects in all regions. The elliptical model, max circle model, and min circle model are all independent of the pattern in question, but the LECD model is pattern dependent [cf. (11) and (15)], so the defect size distribution obtained by using LECD model is also dependent on the pattern concerned. Then the defect number predicted in a region by using LECD model will vary from layout to layout. Here, the LECD model predicts greater number of defects than the other models (elliptical, max circle, and min circle) in the regions about 7.5 μm, where the defect

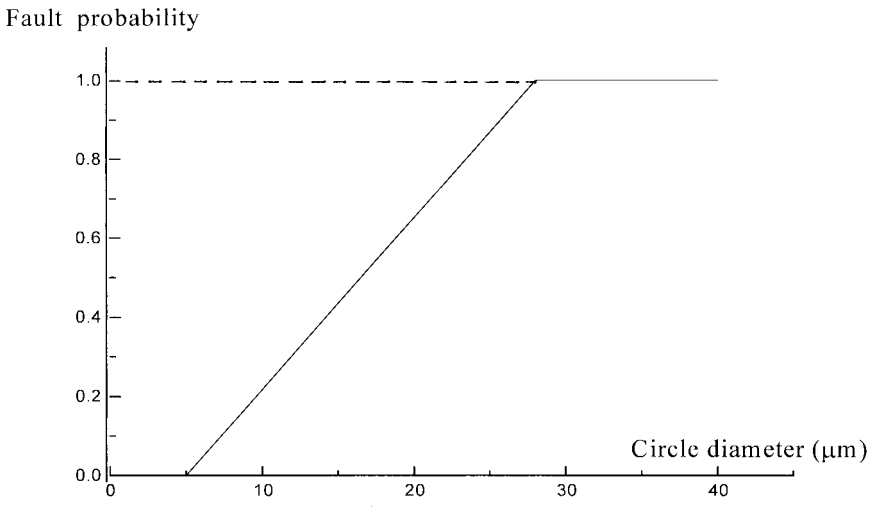

Fig. 7. Fault probability kernel.

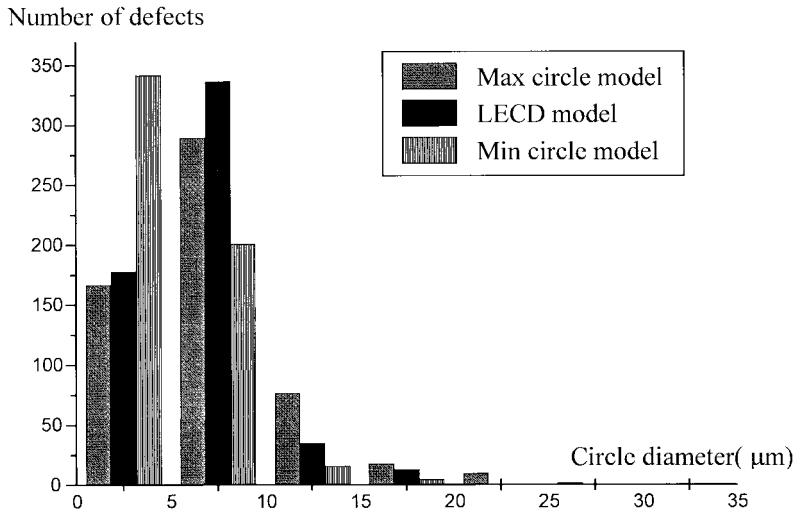

Fig. 8. Measured defect size distribution $(R^*, d_{\max}, d_{\min})$.

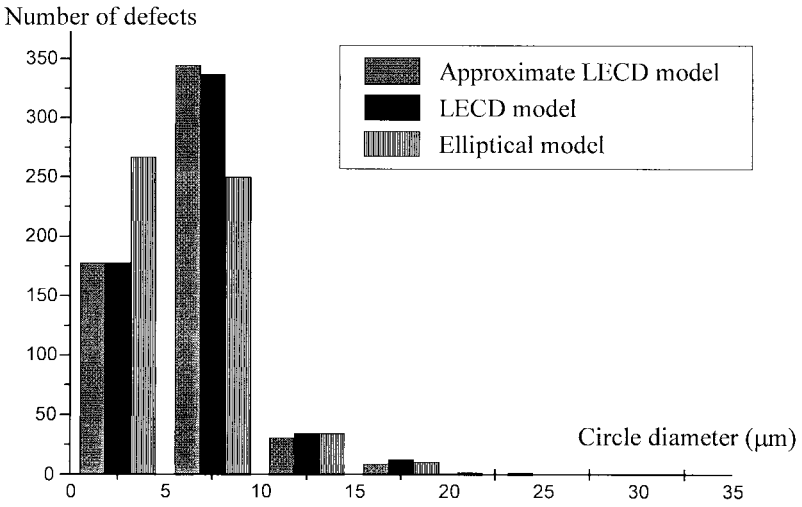

Fig. 9. Measured defect size distribution $(R^*, \hat{R}^*, d_{ellip})$.

TABLE I
COMPARISON OF COMPUTATIONAL TIME FOR DIFFERENT MODELS

Models	d_{max}	d_{min}	d_{ellip}	R^*	$\hat{R}^*$
Computational time per defect (s)	0.4109	0.4109	0.5630	0.5629	0.5637

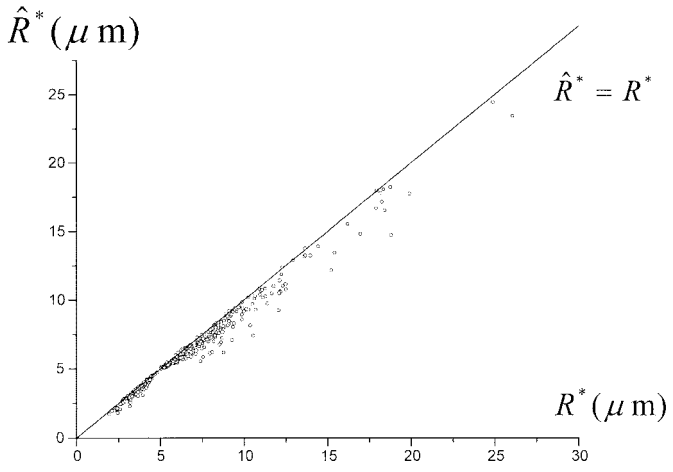

Fig. 10. Plot of R^* versus $\hat{R}^*$.

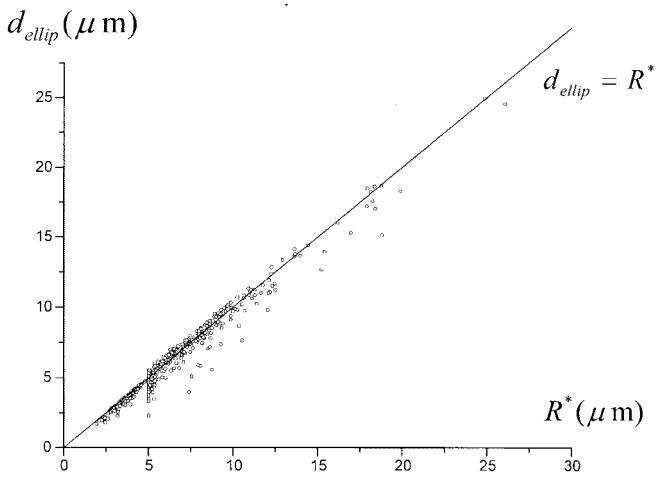

Fig. 11. Plot of R^* versus d_{ellip}.

size distribution obtained by using LECD model reach its peak. In other regions of defect size, however, such is not the case. The LECD model can transform a real defect into a circular defect with just the same probability of causing an open line or a short circuit on the pattern concerned. Thus the probability that a real defect causes a fault in the pattern can be precisely predicted by using the LECD model. Figs. 8 and 9 indicate that there exist great differences between the size distribution of LECD model (or approximate LECD model) and the size distributions of the other models (max circle model, the min circle model, and elliptical model), but the approximate LECD model is almost coincident with the LECD model. Then great errors will be aroused in the prediction of fault probability by using the max circle model, min circle model, and elliptical model. To illustrate the differences furthermore, Figs. 10–13 present the plots of R^* versus $\hat{R}^*$, R^* versus d_{ellip}, R^* versus $d_{\max}$, and R^* versus $d_{\min}$, respectively, and the differences of computational time of the different models are given in Table I.

B. Discussion

The above analysis shows that the LECD model can transform a real defect into a circular defect with just the same probability of causing an open line or a short circuit on the pattern concerned. The distribution of R^* represents the size distribution that should be such that the probability a real defect causes a fault in the pattern can be precisely predicted by using a circular defect model (e.g., max circle model, the min circle model and elliptical model). For a fixed design, the distribution of its R^* provides us a norm to determine the error

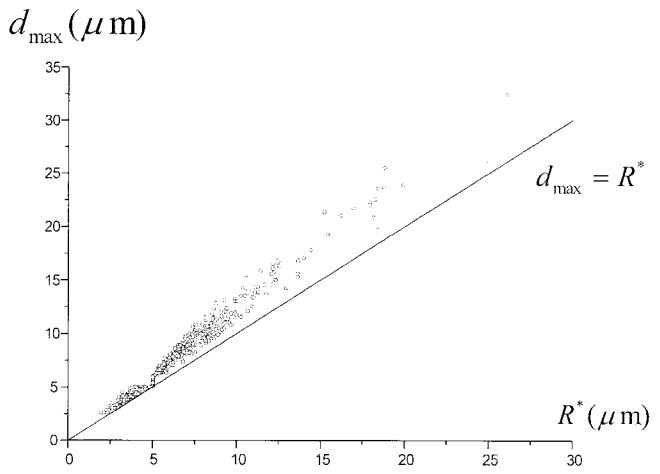

Fig. 12. Plot of R^* versus $d_{\max}$.

that will be aroused in the prediction of the probability a real defect causes a fault in the pattern by using a circular defect model, and thus provides us a norm to estimate approximately the error that will be aroused in the prediction of the fault probability of a new designed pattern by using the circular defect model. For a certain process, a carefully designed text structure (e.g., the novel test structure design developed in paper [11]) should be used to collect enough defect data which can be used to determine the distributions of $d_{\max}$, $d_{\min}$, and d_{ellip}, and then the distributions of R^* and $\hat{R}^*$ of the text structure can also be determined. The differences between the distribution of diameter R^* of the text structure and the

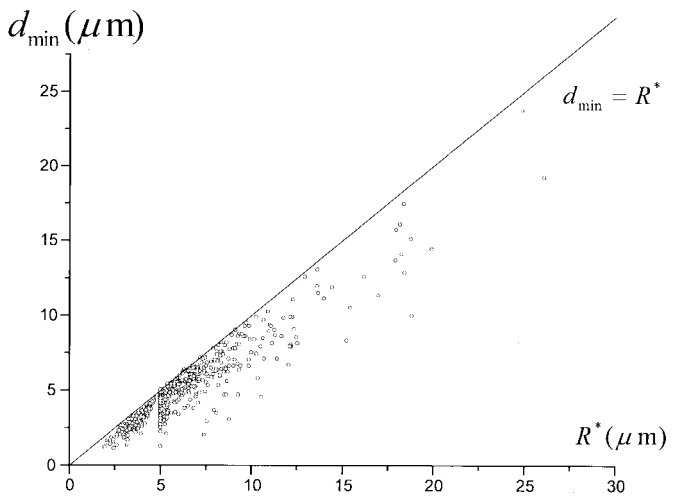

Fig. 13. Plot of R^* versus $d_{\min}$.

distributions of the other diameter ($d_{\max}$, $d_{\min}$, d_{ellip}, and $\hat{R}^*$) will be used for reference in the fault probability prediction (and thus the yield prediction) of a IC's manufactured in the process. Since the R^* is dependent on the pattern in question, R^* may not produce reliable predictions when applied to a new pattern. The results obtained in Figs. 9, 10, and Table I indicate that the $\hat{R}^*$ is almost coincident with R^*, so $\hat{R}^*$ can be used as R^* in practice to eliminate the need to keep all the outline data. The framework developed in this paper takes the defect of type "extra material" as example, but it also applies to other cases where the defect size is concerned.

Although the max circle model, min circle model and elliptical model are simple and pattern independent, but a great number of errors will be aroused in the fault probability prediction of a design (cf. Figs. 8, 9, and 11–13). The actual shape of a defect might be quite complex, but the framework developed in this paper indicates that it is the convex hull of a real defect that is important in determining the probability the defect causes a fault in a pattern. To the extent that this object is less complicated than the actual boundaries, real defect outline model building becomes a more attractive enterprise. Hess and Ströle [11] attempt a good way for the problem. They use $d_{\max}$ and $d_{\min}$ of a real defect to approximate the boundary of the defect by an ellipse which is pattern independent. Our experimental results show that the ellipse is an good approximation to the convex hull of the real defect (cf. Figs. 9 and 10) and it could be used to directly model the defect outlines. These might give rise to more realistic fault probabilities and ultimately yield models, but it is somewhat wasteful to reduce the ellipse in the way proposed by Hess and Ströle (i.e., transform the ellipse into a circle has a diameter of d_{ellip}), especially if the actual outline data has to be maintained to make predictions from layout to layout.

IV. Conclusion

Although the LECD model is pattern dependent and needs high cost for measuring a large number of $d(\theta)$ values, it provides us a norm to determine the accuracy of a defect outline model. The maximum circle model, the minimum circle model, and elliptical model are simple and pattern independent, but they will arouse great errors in the prediction of fault probability of a IC. Thus a great error may be aroused in the estimation of the IC yield. The framework developed in this paper indicates that it is the convex hull of a real defect that is important in determining the probability the defect cause a fault in a pattern, and the ellipse determined by $d_{\max}$ and $d_{\min}$ of a real defect is a good model to approximate the convex hull of the real defect, so it is advocated that the ellipse rather than the maximum circle model, the minimum circle model and elliptical model, should be used for fault probability and yield prediction from layout to layout. The results obtained in this paper lay the foundation for enhancing the accuracy of predicted IC fault probability, and hence enhancing the accuracy of predicted IC yield.

Appendix A
Proof of Theorem 1 (The Existence of LECD)

By the definition of (2), one gets

$$\begin{aligned}
&F_j^o(R, w, s_1, \cdots, s_{n-1}, x)\\
&\quad \in C[X_j, X_{j+1}], \qquad j = 0, 1, 2, \cdots, n-1\\
&F_0^o(X_0, w, s_1, \cdots, s_{n-1}, x)\\
&\quad = n(X_0 - w) - 0 = n(w - w) = 0,\\
&F_{n-1}^o(X_n, w, s_1, \cdots, s_{n-1}, x)\\
&\quad = \frac{1}{x}\left[n(X_n - w) - \sum_{i=1}^{n-1}(X_n - X_i)\right]\\
&\quad = \frac{1}{x}\left[n(s_n + w) - \sum_{i=1}^{n-1}(s_n - s_i)\right]\\
&\quad = \frac{1}{x}\left[n(s_n + w) - (n-1)s_n + \sum_{i=1}^{n-1} s_i\right] = 1\\
&F_k^o(X_{k+1}, w, s_1, \cdots, s_{n-1}, x)\\
&\quad = \frac{1}{x}\left[n(X_{k+1} - w) - \sum_{i=1}^{k}(X_{k+1} - X_i)\right]\\
&\quad = \frac{1}{x}\left[n(X_{k+1} - w) - \sum_{i=1}^{k+1}(X_{k+1} - X_i)\right]\\
&\quad = F_{k+1}^o(X_{k+1}, w, s_1, \cdots, s_{n-1}, x),\\
&\qquad k = 1, 2, \cdots, n-1
\end{aligned}$$

and all in all

$$F^o(R, w, s_1, \cdots, s_{n-1}, x) \in C[0, R_M].$$

From the definition of (1), we know that $F^o(R, w, s_1, \cdots, s_{n-1}, x)$ is a monotonically nondecreasing function in the domain $[X_0, X_n]$. Hence, we also have

$$0 \le F^o(R, w, s_1, \cdots, s_{n-1}, x) \le 1$$

but from (9) and (10), we know that the probability that a real defect causes a fault should hold the following inequality

$$0 \le p^o = \int_0^{\pi} F^o(d(\theta), w, s_1, \cdots, s_{n-1}, x) f(\theta)\, d\theta \le \int_0^{\pi} 1 \times f(\theta)\, d\theta = 1.$$

Then by the intermediate value theorem we know that there exists a $R^* \in [0, R_M]$ such that

$$F^o(R^*, w, s_1, \cdots, s_{n-1}, x) = p^o$$

especially, if

$$0 = F^o(X_0, w, s_1, \cdots, s_{n-1}, x) < p^o < F^o(X_n, w, s_1, \cdots, s_{n-1}, x) = 1$$

then R^* is unique.

Following a similar proof as given above, one can draw a same conclusion for short circuit.

Appendix B
Proof of Theorem 2

From (8), we know that the probability that a real defect falling in the multiple pattern of Fig. 3 causes a short circuit fault can be expressed as

$$\begin{aligned} p^s &= \int_0^{\pi} F^s(d(\theta), w, s_1, \cdots, s_{n-1}, x) f(\theta)\, d\theta \\ &= \int_A F^s(d(\theta), w, s_1, \cdots, s_{n-1}, x) f(\theta)\, d\theta \\ &= \int_{A_0} F^s(d(\theta), w, s_1, \cdots, s_{n-1}, x) f(\theta)\, d\theta \\ &\quad + \int_{A_n} F^s(d(\theta), w, s_1, \cdots, s_{n-1}, x) f(\theta)\, d\theta \\ &\quad + \sum_{j=1}^{n-1} \int_{A_j} F^s(d(\theta), w, s_1, \cdots, s_{n-1}, x) f(\theta)\, d\theta \end{aligned}$$

where

$$\begin{aligned} A &= \{\theta | 0 \le \theta \le \pi\}, \quad A_0 = \{\theta | 0 \le d(\theta) \le s_1\} \\ A_n &= \{\theta | s_n \le d(\theta) \le R_M\}, \\ A_j &= \{\theta | s_j \le d(\theta) \le s_{j+1}\}, \qquad j = 1, \cdots, n-1 \end{aligned}$$

then by the definitions of $F^s(d(\theta), w, s_1, \cdots, s_{n-1}, x)$ and $d(\theta)$ one gets

1) when $\theta \in A_0$, $F^s(d(\theta), w, s_1, \cdots, s_{n-1}, x) = 0$
2) when $\theta \in A_n$, $F^s(d(\theta), w, s_1, \cdots, s_{n-1}, x) = 1$
3) when $\theta \in A_j$, $F^s(d(\theta), w, s_1, \cdots, s_{n-1}, x) = (1/x)[\lambda_j\, d(\theta) + \mu_j]$, $j = 1, \cdots, n-1$,

where λ_j and μ_j are defined in (12) and (13), respectively. Then

$$\begin{aligned} p^s &= \int_A F^s(d(\theta), w, s_1, \cdots, s_{n-1}, x) f(\theta)\, d\theta \\ &= \int_{A_0} 0 \times f(\theta)\, d\theta + \int_{A_n} 1 \times f(\theta)\, d\theta \\ &\quad + \sum_{j=1}^{n-1} \int_{A_j} \frac{1}{x} [\lambda_j\, d(\theta) + \mu_j] f(\theta)\, d\theta \\ &= \sum_{j=1}^{n-1} \frac{1}{x} \left[\lambda_j \int_{A_j} d(\theta) f(\theta)\, d\theta + \mu_j \int_{A_j} f(\theta)\, d\theta \right] \\ &\quad + \int_{A_n} f(\theta)\, d\theta. \end{aligned}$$

Hence, from the conclusion of (3) and the definition of LECD, we know that R^* should hold by the following equation:

$$\begin{aligned} &F^s(R^*, w, s_1, \cdots, s_{n-1}, x) \\ &\quad = p^s = \sum_{j=1}^{n-1} \frac{1}{x} \left[\lambda_j \int_{A_j} d(\theta) f(\theta)\, d\theta + \mu_j \int_{A_j} f(\theta)\, d\theta \right] \\ &\quad + \int_{A_n} f(\theta)\, d\theta. \end{aligned}$$

Acknowledgment

The authors would like to acknowledge D. Xu for advice concerning the programming.

References

[1] F. J. Ferguson and J. P. Shen, "Extraction and simulation of realistic CMOS faults using inductive fault analysis," presented at 1988 Internat. Test Conf..
[2] C. H. Stapper, "On yield fault distributions and clustering of particles," *IBM J. Res. Develop.*, vol. 30, no. 3, May 1986.
[3] A. V. Ferris Prabhu, "Modeling the critical area in yield forecasts," *IEEE J. Solid-State Circuits*, vol. SC-20, pp. 874–878, Aug. 1985.
[4] W. Lukaszek, W. Yarbrough, T. Walker, and J. Meindl, "CMOS test chip design for process problem debugging and yield prediction experiments," *Solid-State Technol.*, vol. 29, no. 3, pp. 87–93, Mar. 1986.
[5] G. Spiegel and A. P. Stroele, "Optimization of deterministic test sets using an estimation of product quality," in *Asian Test Symp.*, Bejing, China, Nov. 1993.
[6] C. H. Stapper, "Modeling of integrated circuit defect sensitivities," *IBM J. Res. Develop.*, vol. 27, no. 6, pp. 549–557, Nov. 1983.
[7] ——, "Modeling of defects in integrated circuits photolithographic patterns," *IBM J. Res. Develop.*, vol. 28, no. 4, pp. 461–474, July 1984.
[8] W. Maly, "Computer-aided design for VLSI circuit manufacturability," *Proc. IEEE*, vol. 78, pp. 356–392, Feb. 1990.
[9] T. L. Michalka, R. C. Varshney, and J. D. Meindl, "A discussion of yield modeling with defect clustering, circuit repair, and circuit redundancy," *IEEE Trans. Semiconduct. Manufact.*, vol. 3, Aug. 1990.
[10] J. P. de Gyvez and D. Chennian, "IC defect sensitivity for footprint type spot defects," *IEEE Trans. Computer-Aided Design*, vol. 11, pp. 638–658, May 1992.
[11] C. Hess and A. Ströle, "Modeling of real defect outlines and parameter extraction using a checkerboard test structure to localize defects," in *IEEE Trans. Semiconduct. Manufact.*, vol. 7, pp. 284–292, Aug. 1994.

Xiaohong Jiang was born in Shaanxi, China, in 1966. He received the B.S. and M.S. degrees in applied mathematics from Xidian University, Xi'an, China, in 1989 and 1992, respectively. Since 1995, he has been pursuing the Ph.D. degree in semiconductor device and microelectronics at Xidian University.

His current research interests include design for VLSI manufacturability, defect modeling, and defect simulation in semiconductor manufacturing process.

Yue Hao (SM'94) was born in Chongqing, China, in 1958. He received the M.S. degree in semiconductor device and microelectronics from Xidian University, Xi'an, China, in 1985, and the Ph.D. degree in computational mathematics from Xi'an Jiaotong University in 1991.

Since March 1991, he has been with Microelectronics Institute of Xidian University, where he is a Professor and Vice President of Xidian University. His research interests are in design for VLSI manufacturability, design for reliability, statistical model and optimization for device and process, and CAD/CAM of ASIC. He has published four books and more than 80 papers.

Dr. Hao is a Senior Member of CIE. He has received various awards and honors, including the Excellent Young Scholar of Shaanxi Province in 1990 and the Contributory Expert Prize of the Ministry of Electronics Industry, China, in 1991.

Guohua Xu was born in Zhejiang, China, in 1937. He graduated from Beijing University, China, in 1961.

He is now a Professor at Xidian University, Xi'an, China. His research interests include SIM and system engineering.